THE ASTROPHYSICAL JOURNAL, 434:484–492, 1994 October 20

THE *HST* QUASAR ABSORPTION LINE KEY PROJECT. IX. AN EMISSION-LINE STUDY OF PG 2251+113[1]

BRIAN R. ESPEY,[2,3] DAVID A. TURNSHEK,[2] LINCOLN LEE,[2] JACQUELINE BERGERON,[4] ALEC BOKSENBERG,[5]
GEORGE F. HARTIG,[6] BUELL T. JANNUZI,[7,8] W. L. W. SARGENT,[9] BLAIR D. SAVAGE,[10]
DONALD P. SCHNEIDER,[7] RAY J. WEYMANN,[11] AND ARTHUR M. WOLFE[12]

Received 1993 November 3; accepted 1994 April 27

ABSTRACT

We present *HST* and quasi-simultaneous ground-based observations of the $z = 0.3252$ QSO PG 2251+113. We find a correlation between line widths and the critical density for de-excitation of the forbidden emission lines observed in this object. We can show that this correlation also applies to the semiforbidden and possibly also the permitted lines which arise in the broad emission-line region. While this result was predicted from statistical studies, it has never previously been shown to hold in detail in any individual object. This relationship between the narrow and broad emission-line regions may help constrain dynamical models of both regions. We examine the implications of this result for a simple radial infall model of the emitting gas developed to explain the origin of narrow-line profiles.

Subject headings: quasars: absorption lines — quasars: individual (PG 2251+113) — ultraviolet: galaxies

1. INTRODUCTION

PG 2251+113 (4C 11.72, OY 186, MRC 2251+113, PKS 2251+11) is a steep-spectrum weak radio source with extended narrow-line emission and a disturbed velocity field at large distances from the nucleus (Crampton & Hutchings 1990). UV and optical data have been obtained within 5 days of each other and analysis of the data provide information on the physical conditions of the emission line producing regions in the spectrum. By far the most interesting result of this work is the discovery of a correlation between line width and the region of highest density where peak line emission is produced. Such a correlation has been shown to hold over a range of lower densities in a number of lower luminosity objects (Pelat, Alloin, & Fosbury 1981; Filippenko & Halpern 1984; Filippenko 1985; Appenzeller & Östereicher 1988) and indications of a similar relationship have been seen in objects of comparable or marginally higher luminosity (Appenzeller & Wagner 1991). However, our observations directly demonstrate, rather than infer, the extension of this relationship into the broad emission-line region (BELR) itself using data from semiforbidden and permitted lines. The result supports models in which the BELR and narrow emission-line region (NELR) are connected by a "transition emission-line region" (TELR). The transition region is generally difficult to study because of the paucity of indicators for the density and ionization levels postulated. The presence of a continuous range of properties between the two regions has important implications for models of active galactic nuclei (AGN) as NELR cloud motions are easier to determine and the region is generally easier to study. This work illustrates the importance of the *HST* for the study of low-redshift AGN emission lines and for AGN models in general.

2. DATA SET

UV data were obtained with the *HST* Faint Object Spectrograph (FOS) and the G270H, G190H, and G130H gratings during the Quasar Absorption Line Key Project. The G270H and G190H data have been presented by Bahcall et al. (1993) and details are given there. The G130H data were obtained about a half-year later, but comparison of these data with those of the G160L spectrum obtained at the same epoch as the G190H and G270H data suggest that there was no noticeable change in brightness between these times. Optical data which were nearly contemporaneous (5 day time difference) with the G270H and G190H data were obtained using the Ritchey-Chrétien spectrograph on the KPNO 4 m telescope. We mention here for completeness that the data have a resolution of ~ 2 Å in the observed frame from UV wavelengths to 4875 Å, and about half this resolution for longer wavelengths. A journal of observations for all the data is given in Table 1.

The UV data were processed as outlined by Schneider et al. (1993) who also describe how interstellar absorption features were used to align the wavelength scales of the individual spectra to an interstellar medium (ISM) reference frame. The difference between the heliocentric and the galactic absorption system velocity amounts to only 22 km s^{-1} (see Savage et al. 1993 for details). This wavelength offset is much smaller than

[1] Based on observations made with the NASA/ESA *Hubble Space Telescope*, obtained at the Space Telescope Science Institute, which is operated by the AURA, Inc., under NASA contract NAS 5-26555, and with the NOAO KPNO 4 m telescope, which is operated by AURA, Inc., under agreement with NSF.

[2] Department of Physics and Astronomy, University of Pittsburgh, Pittsburgh, PA 15260.
[3] Now at Center for Astrophysical Sciences, Johns Hopkins University, Baltimore, MD 21218.
[4] Institut d'Astrophysique de Paris, CNRS, 98 bis Boulevard Arago, F-75014 Paris, France.
[5] Royal Greenwich Observatory, Madingley Road, Cambridge CB3 0EZ, England, UK.
[6] Space Telescope Science Institute, 3700 San Martin Drive, Baltimore, MD 21218.
[7] Institute for Advanced Study, School of Natural Sciences, Princeton, NJ 08540.
[8] Hubble Fellow.
[9] Mail Code 105-24, California Institute of Technology, Pasadena, CA 91125.
[10] Department of Astronomy, University of Wisconsin, Madison, WI 53706.
[11] OCIW, 813 Santa Barbara Street, Pasadena, CA 91101.
[12] CASS, University of California San Diego, La Jolla, CA 92093.

TABLE 1

JOURNAL OF SPECTROSCOPIC OBSERVATIONS

Telescope	Instrument	UT Date	Exposure Time (s)	Coverage (Å)	Resolution (Å)
HST	FOS G190H	1991 Oct 23	4000	1565–2310	1.5
HST	FOS G270H	1991 Oct 23	1200	2230–3280	2.1
KPNO 4 m	RC spectrograph + TEK CCD	1991 Oct 27	1800	3195–3975	2.0
KPNO 4 m	RC spectrograph + TEK CCD	1991 Oct 27	1200	3195–3970	2.0
KPNO 4 m	RC spectrograph + TEK CCD	1991 Oct 27	1200	4875–6395	4.0
KPNO 4 m	RC spectrograph + TEK CCD	1991 Oct 27	1200	6105–7635	4.0
KPNO 4 m	RC spectrograph + TEK CCD	1991 Oct 28	300	3195–3975	2.0
KPNO 4 m	RC spectrograph + TEK CCD	1991 Oct 28	600	3925–4700	2.0
KPNO 4 m	RC spectrograph + TEK CCD	1991 Oct 28	600	4610–6130	4.0
KPNO 4 m	RC spectrograph + TEK CCD	1991 Oct 28	1200	6000–7530	4.0
HST	FOS G130H	1992 Apr 12	16000	1150–1606	1.1

the resolution of our optical ($\gtrsim$150 km s^{-1}), or *HST* ($\approx$180 km s^{-1}) data in the AGN's rest frame and is approximately the same as the rms wavelength calibration error. We have thus chosen to ignore this difference in the following analysis.

The optical data cover the observed wavelength interval 3260–7240 Å and were obtained with the spectrograph slit at the parallactic angle. Flux calibration was performed by obtaining data for both object and standard stars using a 10 arcsec wide slit. The data were processed and calibrated using IRAF[13] software and standard reduction techniques. Due to equipment problems, data extending redward of the Hα region were not obtained. Because the object is variable (see § 3), we elected not to extend our optical spectra with longer wavelength data taken at a substantially earlier epoch.

Figures 1*a* and 1*b* present the complete spectrum covering from the UV to red wavelength regions together with an underlying power-law continuum fit which was chosen to pass through line-free emission regions similar to those listed by Kallman et al. (1993). In addition we have included those points unaffected by atmospheric absorption lying between 5400–6200 Å which have been defined as line-free by Wills, Netzer, & Wills (1985). Inspection of the continuum fit suggests the presence of a strong UV component of Fe II emission. There is evidence for a real decrease in the continuum emission shortward of the Lyα line relative to the power-law extrapolation. We believe, however, that while this falloff provides evidence for a more complicated continuum shape (perhaps an accretion disk), the power-law continuum we have illustrated has the merit of simplicity. The power-law continuum also appears to provide a good fit to the region longward of Lyα with the possible exception of two regions near C IV for which we believe the 2200 Å Galactic extinction feature may have been marginally undercorrected.

[13] IRAF is distributed by NOAO, which is operated by AURA, Inc., under contract to the NSF.

3. VARIABILITY AND EXTRANUCLEAR EMISSION

PG 2251+113 has been observed to be variable by Pica & Smith (1983) who detected variations up to ~0.4 mag with a time baseline extending over 13 yr. Comparison of our data with the published optical spectra for this object shows that both the lines and continuum vary on an observed timescale of years, although this period is not well-defined due to a lack of

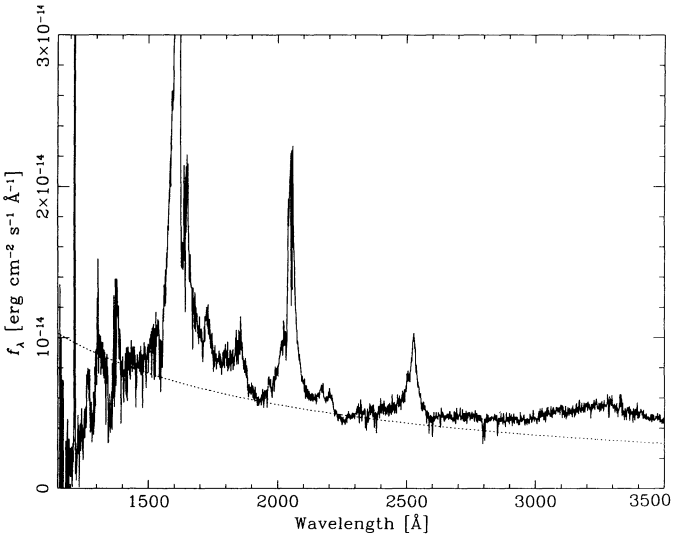

FIG. 1*a*

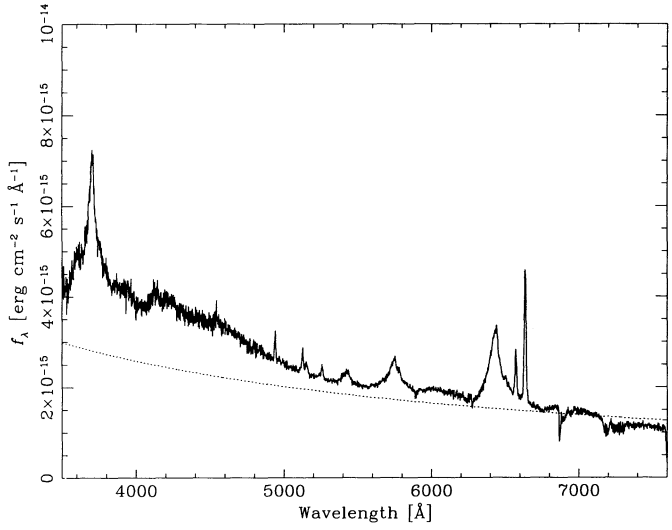

FIG. 1*b*

FIG. 1.—(*a*, *b*) Combined *HST* FOS and KPNO 4 m data for PG 2251+113. The absorption longward of 6800 Å is due to incomplete cancellation of the telluric absorption by the Fraunhofer *A* and *B* bands.

sufficient time coverage. Furthermore, the data of Angione et al. (1981) raise the possibility that the source may be variable on a timescale of months.

Figures 2*a* and 2*b* show our data compared to data obtained by others at different epochs. To facilitate direct comparisons and to enable the difference spectra to be formed, the original data were smoothed and rebinned to a uniform scale. The spectra shown have been scaled to correct for differences in observing procedure and seeing by normalizing the total of the [O III] $\lambda\lambda$4959, 5007 fluxes to a common value. The [O III] fluxes were determined by fitting a power law to the redwing of the Hβ emission-line profile and then determining the best-fit [O III] fluxes by constraining the line components to have the 1:3 flux ratio required by atomic physics. Both the optical data presented in this paper and those of Boroson & Green (1992) were taken at, or near, the parallactic angle so the slits should cover the same region of the object. The data of Stirpe (1990), however, were obtained with the slit in an east–west direction and so may contain a component from the extended line emission discussed by Crampton & Hutchings (1990)—see their Figure 9. Stockton & MacKenty (1987) estimated that the extended [O III] 5007 emission strength is one-third that of the nuclear component. Most of this emission is concentrated in a bright knot $\approx 4''$ southeast of the nucleus. Comparison of the data in the figure indicates that the spectrum which we have obtained is consistent with that obtained by Boroson & Green

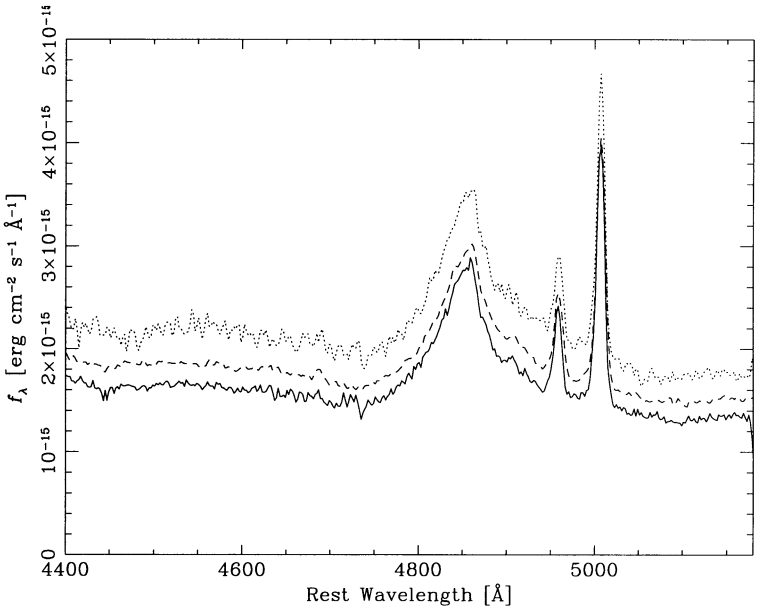

FIG. 2*a*

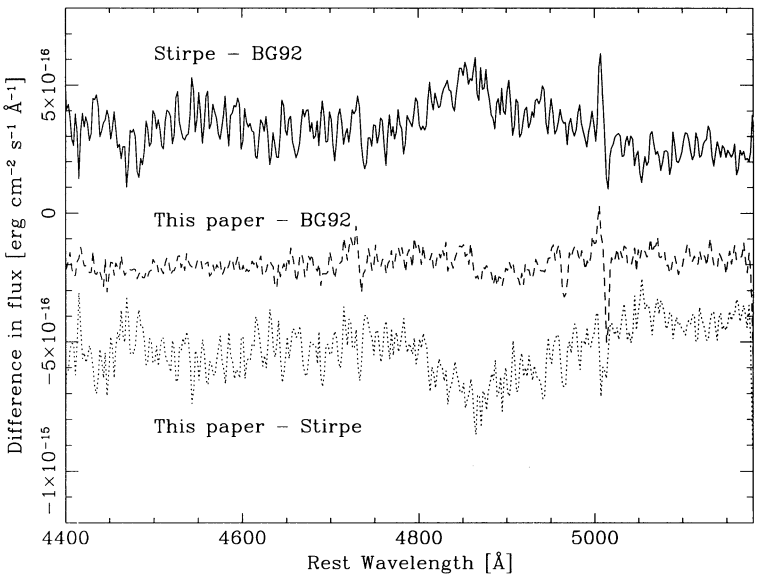

FIG. 2*b*

FIG. 2.—(*a*, *b*) The Hβ region of the spectra showing changes in both the continuum and line strengths. In 2*a* we show the available spectra normalized to the same total [O III] λ4959 + 5007 line flux. From top to bottom the data are from Stirpe (1990), Boroson & Green (1992), and this paper. Figure 2*b* shows the difference data for these spectra. Note that there is comparatively little variation in the Fe II lines relative to the Hβ component.

while the Stirpe data contains an Hβ component of ~7000 km s^{-1} which may be due to the excess emission to the east of the nucleus noted by Crampton & Hutchings (1990).

These considerations imply that analysis of the spectrum is best carried out with multiwavelength data taken as close as possible in time.

4. OPTICAL STRUCTURE OF THE OBJECT

PG 2251+113 was imaged by Stockton & MacKenty (1987) and they noted the presence of extended clumpy [O III] emission, most of which was associated with the radio lobes. Long-slit spectra obtained by Crampton & Hutchings (1990) showed that the velocities of the [O III] "blobs" indicate the presence of a chaotic velocity field and the possibility of some scattered nuclear light. Their observed upper limit on the ratio [O III] λ5007/[O III] λ4363 > 15 for the "blobs" places an upper limit on the gas temperature $T_e < 3.2 \times 10^4$ K. This limit is lower if the gas density $n_e \gtrsim 10^3$ cm^{-3}. There is no evidence in the recent imaging data of Hutchings & Neff (1992) for interaction of the host galaxy with any nearby object, hence the gas cloud dynamics are probably dominated by local processes.

As noted in § 2, our optical spectra were obtained with the slit at the appropriate parallactic angles to minimize atmospheric losses and all spectra were taken close to the time of meridian transit. A further advantage of the slit angles used was that they lay roughly perpendicular to the axis of the radio lobes and thus contamination of our data by extranuclear line flux should be minimal. This is confirmed by the observed width of the spectra in the spatial direction of ≈2.″5 (≈3.5 kpc for $H_0 = 50$ km s^{-1} Mpc^{-1}), consistent with the seeing at the time. In particular, comparison of the Hβ and [O III] profiles shows no indication of an extended component. Although the *HST* data were obtained using the 0.″25 × 1.″4 slit, the position angles used suggest that any contamination of the nuclear UV fluxes by the extended emission component should be minimal.

5. EMISSION-LINE PROFILES

The emission-line profiles were fitted using Kriss's SPECFIT software which is available in the STSDAS.CONTRIB section of the IRAF software (Kriss 1994). The SPECFIT software contains a number of possible models which may be used to parameterize spectral data, and a choice of either a simplex or a Marquardt χ^2 minimization algorithm for the fitting. The Marquardt algorithm proved to be too sensitive to initial conditions, but is better for optimization close to a minimum in parameter space. We therefore adopted the method of using the simplex algorithm first and then switching to a Marquardt approach to refine the parameters further.

The emission-line profiles were isolated by defining a local continuum with a power-law fit using line-free regions within a few hundred angstroms on either side of each line and then subtracting the local continuum. The profiles were then fitted using multiple components to account for lines arising in different emitting regions, with the flux and width as free parameters for each component. For the narrowest lines a symmetric Gaussian profile proved sufficient, but for the broader lines two components consisting of a broad Gaussian profile and a broader power-law profile were necessary. The measurements are presented in Table 2. The narrow component is designated "N" and the broad Gaussian and broader power-law components are designated "B1" and "B2," respectively. The B1 component may be identified with material which has random line-of-sight velocities, such as clouds in a spherical distribution which move predominantly under Keplerian motion and the B2 component with, for example, an outflowing disklike distribution of matter (see Zheng 1992; van Groningen 1983, and references therein).

TABLE 2A

LINE MEASUREMENTS FOR PG 2251+113

Transition	Component	Observed Wavelength (Å)	FWHM (km s^{-1})	Line Flux (ergs cm^{-2} s^{-1})
Lyα 1216	N	1611.9	2746	8.76×10^{-13}
Lyα 1216	B1	1598.2	7669	5.96×10^{-13}
Lyα 1216	B2	1600.6	28426	6.83×10^{-13}
	tot			2.16×10^{-12}
N v 1240	B1	1646.7	3423	1.75×10^{-13}
N v 1240	B2	1640.1	18047	1.10×10^{-14}
	tot			1.86×10^{-13}
Si II 1263		1679.7	11773	1.98×10^{-13}
O I 1304		1730.3	3905	7.16×10^{-14}
?		1784.1	15311	1.96×10^{-13}
Si IV 1394	B1	1854.4	3153	2.01×10^{-14}
Si IV 1402	B1	1866.4	3153	9.97×10^{-15}
	tot			3.01×10^{-14}
Si IV 1394	B2	1848.7	18394	3.43×10^{-14}
Si IV 1402	B2	1860.6	18394	1.70×10^{-14}
	tot			5.13×10^{-14}
O IV] 1402		1850.7	8703	1.03×10^{-13}
N IV] 1486		1967.0	1909	1.81×10^{-14}
C IV 1549	B1	2053.5	2963	2.86×10^{-13}
C IV 1549	B2	2043.9	11959	4.47×10^{-13}
	tot			7.33×10^{-13}
He II 1640	B1	2170.6	2009	1.03×10^{-14}
He II 1640	B2	2163.9	4907	9.29×10^{-15}
	tot			1.96×10^{-14}
O III] 1663		2200.7	1533	7.76×10^{-15}

In the optical data set the existence of regions of low-amplitude, complex Fe II emission is apparent (Figs. 1*a*–1*b*). Therefore, we measured the emission lines relative to locally defined continuua, but we used the power-law fit shown in Figures 1*a* and 1*b* and a fit to the Fe II emission to assess possible problems. We followed the methods of Phillips (1978) and Boroson & Green (1992) for generating a best-fit Fe II spectrum using Boroson & Green's observations of the narrow-line Seyfert I Zw1 (T. A. Boroson, private communication). A series of templates was generated by broadening the I Zw1 Fe II lines by differing amounts. The best fit was obtained using the SPECFIT program which interpolated and scaled these templates until a good match to the PG 2251+113 data was obtained.

A problem experienced with some narrow emission lines was how to deblend them when they were severely blended with adjacent broad lines. As an example, the Hε and Hζ profiles are blended with the [Ne III] λλ3968, 3869 and [S II] λλ4069, 4076 lines, respectively. For these doublets which have components which arise from a common upper atomic level we fixed the ratios to the values prescribed by their branching ratios. The doublets of [Ne III] λλ3968, 3869 and [O III] λλ4959, 5007 were handled in this fashion. For lines which are sensitive to density and/or temperature, we fitted the profiles

TABLE 2B

LINE FLUXES FOR PG 2251+113

Transition	Component	Observed Wavelength (Å)	FWHM (km s^{-1})	Line Flux (ergs cm^{-2} s^{-1})
Al III 1857	B1	2451.9	7697	3.86×10^{-15}
Al III 1857	B2	2461.3	8467	1.52×10^{-14}
	tot			1.91×10^{-14}
Si III] 1892	B1	2507.2	2409	5.24×10^{-15}
Si III] 1892	B2	2497.7	6545	2.59×10^{-14}
	tot			3.11×10^{-14}
[C III] 1907	N	2528.4	1480	3.10×10^{-14}
C III] 1909	B1	2527.1	4712	6.38×10^{-14}
C III] 1909	B2	2519.7	5777	4.21×10^{-14}
	tot			1.37×10^{-13}
Mg II 2798	N	3712.4*	731	4.82×10^{-15}
Mg II 2798	B1	3705.4*	3540	1.59×10^{-13}
Mg II 2798	B2	3697.0*	4917	1.93×10^{-13}
	tot			3.57×10^{-13}
[O II] 3726		4937.7	543	2.84×10^{-15}
[O II] 3729		4941.3	543	3.20×10^{-15}
[Ne III] 3869		5126.5	774	6.47×10^{-15}
[Ne III] 3968		5257.4	774	1.98×10^{-15}
Hζ 3889	N	5149.9	674	1.51×10^{-15}
Hζ 3889	B1	5158.4	2139	9.38×10^{-15}
Hζ 3889	B2	5164.3	3399	2.00×10^{-16}
	tot			1.11×10^{-14}
Hε 3970	N	5264.2	674	2.38×10^{-16}
Hε 3970	B1	5257.6	2139	1.23×10^{-14}
Hε 3970	B2	5240.3	3399	7.83×10^{-16}
	tot			1.33×10^{-14}
[S II] 4069		5392.3	676	8.11×10^{-16}
[S II] 4076		5402.6	676	7.76×10^{-16}
Hδ 4102	N	5436.5	674	1.68×10^{-15}
Hδ 4102	B1	5427.1	2139	1.60×10^{-14}
Hδ 4102	B2	5419.3	3399	1.04×10^{-14}
	tot			2.81×10^{-14}
Hγ 4340	N	5752.9	674	3.93×10^{-15}
Hγ 4340	B1	5743.0	2139	2.55×10^{-14}
Hγ 4340	B2	5734.7	3399	3.77×10^{-14}
	tot			6.71×10^{-14}
[O III] 4363		5779.6	1580	7.55×10^{-15}
Hβ 4861	N	6443.2	674	6.90×10^{-15}
Hβ 4861	B1	6432.1	2139	1.64×10^{-14}
Hβ 4861	B2	6422.8	3399	1.86×10^{-13}
	tot			2.09×10^{-13}
[O III] 4959		6572.2	645	1.43×10^{-14}
[O III] 5007		6635.7	645	4.30×10^{-14}

NOTES.—Component identification: N = narrowest component; B1 = narrower (Gaussian) broad component; B2 = broadest (power-law) broad component.

Where no component is indicated a single Gaussian fit was used. Asterisk (*) tied to relevant Balmer line values.

Line fluxes have been measured from the extinction corrected spectrum assuming a Galactic $E(B-V) = 0.098$.

by tying the line ratios in turn to their low and high-density limits. The line width of each component was left free in each case and the derived FWHM was compared to the result obtained when the line fluxes were also allowed to be free parameters. The adopted line width and error were determined by comparing derived values and χ^2 statistics of these fits.

Fitting of the Balmer lines was facilitated by tying the line widths and redshifts of similar components (e.g., the N, B1, or B2) of all Balmer lines together. This process is probably not accurate in detail as some differences in line width through the Balmer series have been observed in other AGN, but it proved necessary to apply some form of constraint to the line widths in order to simplify the deblending procedure. The Balmer lines up to Hε were fitted directly with constraints to have similar line widths and shapes as discussed above. Figure 3 shows an illustrative example of line deblending for the region near Hβ. For this plot we used a Fe II template provided by Hagai Netzer (private communication) as it covered a wider wavelength range than that of Boroson & Green (1992).

6. DISCUSSION

From Table 2 we see that there are systematic velocity shifts between the centroids of the narrow component of each line fit (designated N in the table) and the two components representing the broad-line region (designated B1 and B2), but no pronounced velocity differences between lines from different ions are seen to the limit of our resolution ($\delta v \sim 200$ km s^{-1}). Also listed in Table 2 are the emission-line fluxes, which have been corrected for Galactic extinction of $E(B-V) = 0.098$ based on recent HI 21 cm observations of Lockman & Savage (1993) together with the conversion of $E(B-V) = N(\text{H I})/5.53 \times 10^{21}$ cm^{-2} which is appropriate for low column density sight lines (Diplas & Savage 1993). This value is higher than the value of ≈ 0.037 used by previous authors based on the results of Burstein & Heiles (1978), but their column density estimates appear to be biased to lower values (Falomo et al. 1993). The extinction value we derived is also higher than that implied by the A_B data in the NED database, which seems to be based on the Burstein & Heiles results.

Our ground-based data were flux-calibrated and matched with each other in the overlap regions before being scaled to match the flux in the overlap region of the *HST* data. The *HST* calibration should be accurate to $\approx 10\%$ although there is the possibility of some light loss due to miscentering of the target in the aperture. Trials using different functional forms (e.g., Gaussian or power-law) for the components of an individual line profile suggest that the total line flux measurements are repeatable to the $\approx 10\%$ level. The accuracy of the flux and shape determination of individual components of a blended emission line is dependent on a number of parameters among which are signal-to-noise, number of blended lines, and degree of blending and hence varies from profile to profile. Errors in the extinction-corrected line fluxes are also possible due to uncertainties in the assumed dust-to-gas ratio along our line of sight, particularly in the region near the C IV line as this lies close to the 2200 Å Galactic extinction feature (see § 2).

6.1. *The Narrow Emission-Line Region (NELR)*

We derive $z_{\text{NELR}} = 0.3252$ from a weighted fit to the least blended optical emission lines of [Ne III] λ3968, [O II] λ3729, [O III] λ5007 and Hβ λ4861. This value is consistent with the value of 0.3253 ± 0.003 reported by Crampton & Hutchings (1990).

The fluxes determined for lines arising in the NELR include the density and temperature-dependent lines of [O II] λ3727 and [O III] λλ4363, 4959, 5007. Gaussians were found to provide good fits to the observed line profiles and no pronounced velocity shifts were found between the various lines at the limit of our resolution of ~ 200 km s^{-1}. From the reddening-corrected line fluxes listed in Table 2, the estimated apparent average density and temperature in the region forming the majority of the [O II] and [O III] line flux is

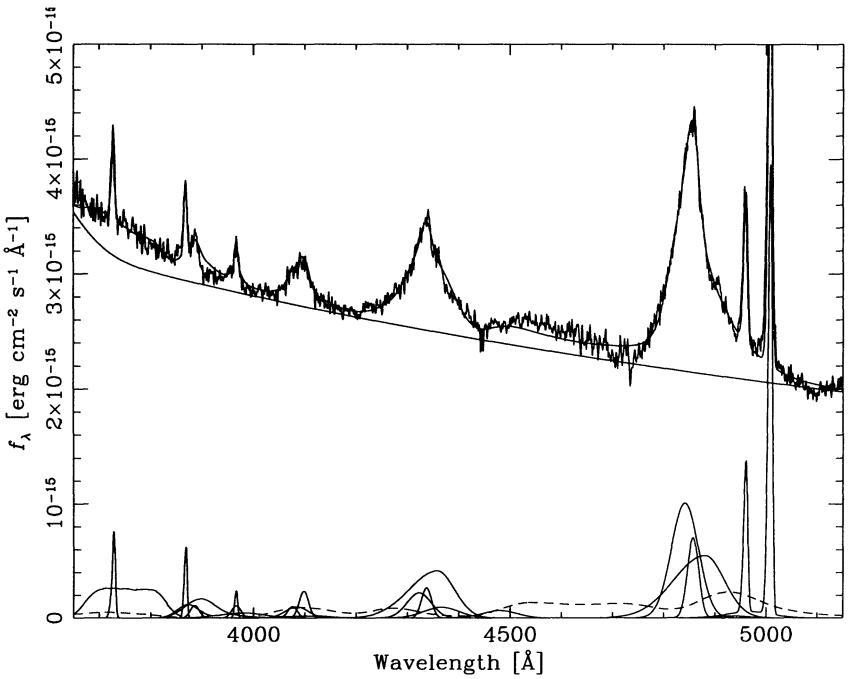

FIG. 3.—An example of line deblending is shown for the region between Hδ and Hβ. The sum of the components is shown superposed on the data; the various emission-line components are plotted underneath. The sharply peaked profiles are the power-law (B2) components. The narrow and B1 components are represented by symmetric Gaussians.

$n_e \simeq 750$ cm^{-3} and $T_e \simeq 5 \times 10^4$ K, respectively. The derived temperature is high and could be considered indicative of shock heating in the NELR but, as has been pointed out by Filippenko (1985), the presence of density stratification within the NELR (see § 6.4) may mimic the effect of high temperatures when line fluxes are determined by simple integrating under the line profile. In the case of PG 2251−178, which is of roughly comparable luminosity to the object studied here, Filippenko found that the density varied by over an order of magnitude across the emission-line region. The contribution of the high-density gas to the line fluxes suggests that the temperature and density derived from the oxygen lines be taken as upper and lower limits respectively to the regions producing these emission lines.

6.2. *Line Widths and Density Correlation*

The observed line widths and the critical densities for de-excitation of each observed forbidden and semiforbidden emission lines are listed in Table 3 and illustrated in Figure 4. The listed values are the mean values derived from independent fits performed by two of us (B. R. E. and L. L.). In the case of lines blended with broad emission lines, we assumed a different shape for the broadest component (the B2 component) to ensure that the derived line widths were not too dependent on the assumed line shape. In one case an asymmetric power-law component was assumed (as described in § 5), and for the other an asymmetric Gaussian component was assumed. The quoted error provides an estimate of the repeatability of the measurement process and reflects the difference between the mean and the values determined from each of the independent fits.

A straight-line fit to the data points in Figure 4, excluding the upper limits and the mean data for the BELR permitted lines suggests a relationship of the form: FWHM $\propto n^{0.113}$. Deviations from the linear trend are apparent for the upper limits derived for the blended "[C III] λ1907" and Si IV + O IV] λ1400 lines. The ≈λ1907 line is probably a blend of both NELR [C III] λ1907 and BELR C III] λ1909 components. At the [C III] λ1907 critical density of $\approx 4 \times 10^5$ cm^{-2}, the semiforbidden line of C III] λ1909 is expected to be approximately an order of magnitude stronger based on atomic physics alone (Osterbrock 1989). A NELR model by Ferland

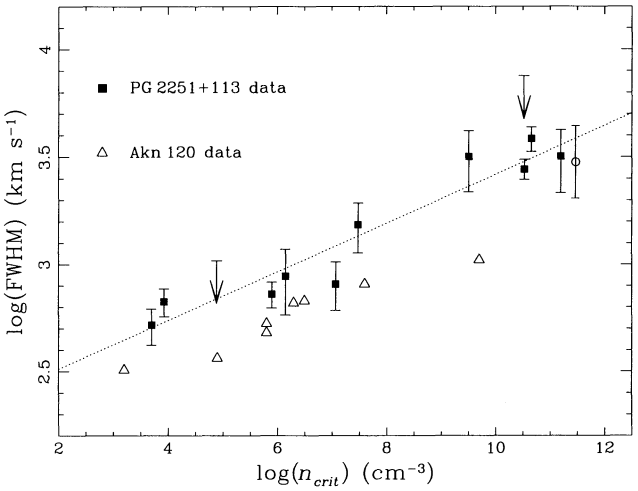

FIG. 4.—Plot showing the correlation between the line widths (corrected for instrumental resolution) and the critical density for de-excitation. Upper limits are shown for cases where the lines are badly blended with adjacent features (e.g. [C III] λ1907 and O IV] λ1402 lines). The open circle at the upper right in the diagram shows the mean line width for the C IV λ1549, Mg II λ2798, and Hβ λ4861 lines plotted at the mean thermalization density appropriate to these lines. Error bars indicate the range of FWHM values found in two independent fits to the data using different assumed component shapes (see text).

TABLE 3

OBSERVED FWHM AND CRITICAL DENSITY VALUES FOR PG 2251+113

log n_cr	FWHM[a] (km s^{-1})	Error	log FWHM	u_err	l_err	Line	WAVELENGTH (Å)	REFERENCE
3.70	520	100	2.716	0.076	0.093	[O II]	3727	1
3.93	670	100	2.826	0.060	0.070	[O II]	3729	1
4.89	1043	200	3.018	0.076	0.092	[C III] N	1907	1
5.90	727	100	2.861	0.056	0.064	[O III]	4959/5007	2
6.15	882	300	2.945	0.127	0.181	[S II]	4069/4076	1
7.07	809	200	2.908	0.104	0.123	[Ne III]	3869/3968	2
7.48	1536	400	3.186	0.101	0.131	[O III]	4363	2
9.51	3177	1000	3.502	0.119	0.164	C III] B1	1909	1
10.52	7508	1000	3.876	0.054	0.062	O IV]	1402	1
10.53	1713	700	3.442	0.047	0.043	N IV]	1486	1
10.66	3846	500	3.585	0.053	0.060	O III]	1663	1
11.2	3092	1000	3.503	0.122	0.170	Si III] B1	1893	3
11.5[b]	2992	860	3.516	0.168	0.168	permitted[c]	1549, 2798, 4861	3

[a] The listed line widths and their errors are estimated from values derived from two independent fits (see text).

[b] Thermalization density.

[c] Mean data for the relatively unblended B1 lines of C IV 1549 Å, Mg II 2798 Å and Hβ 4861 Å.

REFERENCES.—(1) Zheng, W. 1988; (2) Filippenko, A. V., & Halpern, J. P. 1984; (3) Rees, M. J., Netzer, H., & Ferland, G. J. 1989.

(1981), however, suggests that I([C III] λ1907)/I(C III] λ1909) ≈ 1 so it is probable that the narrow line blend contains components from both the forbidden and semiforbidden lines. The observed line is thus probably somewhat broader than expected which is consistent with the measured line width of the narrow feature. Only an upper limit to the width of the ≈λ1400 feature was derived since it was impossible to unambiguously deblend the Si IV and O IV] components.

In addition to results on the forbidden and semiforbidden lines shown in Figure 4 we have also plotted the mean line width of the B1 components of the Hβ, C IV, and Mg II lines which have thermalization densities in the region of $\approx 3 \times 10^{11}$ cm^{-3}. We have done this as the thermalization density is a qualitatively similar phenomenon for permitted lines as is the critical density for forbidden and semiforbidden lines (Rees, Netzer, & Ferland 1989). The location of the mean value in this plot provides some further evidence in favor of high densities in the BELRs of AGN. Corroboration of this comes from comparison of the hydrogen line ratios with those predicted for densities in this range (Drake & Ulrich 1980). Empirical evidence for high-density broad components in other AGN has also been found from studies of emission-line ratios (Marziani & Sulentic 1993) and from studies of AGN variability (Peterson 1993; Ferland et al. 1992).

It would be instructive to study the line widths of lines which probe to higher (thermalization) densities such as the N V λ1240 line ($> 10^{12}$ cm^{-2}), but this line is blended with Lyα and unambiguous determination of its line width is not possible. A similar problem exists for high-excitation lines available in the G130H data. The O VI λ1035 line is blended with Lyβ λ1025 and the C III λ977 feature is a blend with Lyγ λ973 on the blue side and N III λ991 on the red. In addition, these lines are also affected by absorption from both associated and intervening clouds (see Fig. 1*a*). We do, however, have measurements of the He II λ1640 which is expected to thermalize at densities $\gtrsim 3 \times 10^{13}$ cm^{-3}. The observed line width is consistent with those observed for other BELR lines suggesting that densities do not rise much higher than those giving rise to the bulk of the broad emission lines.

A comparison of the results for PG 2251+113 with measurements of the emission lines of Akn 120 published by Appenzeller & Östereicher (1988) is instructive and these later data have been overplotted on Figure 4. There is remarkable agreement between the slopes determined for these two objects despite a factor of ≈2000 difference in luminosity.

6.3. *Continuity of the Emission-Line Regions*

The existence of a smooth trend seen in Figure 4 joining the broad and narrow emission-line regions suggests that there is a continuous range of gas properties with radius. Van Groningen & de Bruyn (1989) have studied line emission from a region which they conclude lies between the conventional NEL [$3 \lesssim \log (n_e) \lesssim 6$] and BEL [$9 \lesssim \log (n_e) \lesssim 11$] regions. Using high signal-to-noise spectroscopy of the [O III] λλ4363, 4959, and 5007 lines, they find that this region has a density of $\approx 5 \times 10^6$ cm^{-3}. A transition line region of this density lies within the region sampled by the emission lines in PG 2251+113, but there is an apparent gap for the range $8 \lesssim \log (n_e) \lesssim 9.5$ due to the lack of emission lines with critical densities in this range.

Netzer & Laor (1993) considered a continuous zone model which was specifically designed to study how an apparent dichotomy in properties between the NELR and BELR might arise. They found that it is possible to suppress emission lines in cases where dust is intimately associated with the emission-line material lying just outside the BELR. From AGN variability studies and recent work on the survivability of dust it is expected that the region beyond the outer radius of the BELR is sufficiently cool that dust may survive. The dust grains have a strong influence on the emissivity of the emission-line clouds and lines such as Hβ are about two orders of magnitude less efficiently produced from this region than from the zone just inside it. The [O III] λ4959, 5007 is even more sensitive to the properties of this region and is suppressed by a factor of $\approx 10^5$ relative to the region of optimum emission due to a combination of dust and density effects. These results suggest one reason why there is no strong permitted or forbidden line emission from this region and hence why no component is observed in the emission-line profile deblending.

Work by Appenzeller & Wagner (1991) indicated that the line widths of the higher ionization [Fe VII] λ6086 ($n_{\rm crit} = 3.0 \times 10^7$ cm^{-3}) and [Ne V] λ3426 ($n_{\rm crit} = 3.7 \times 10^7$ cm^{-3})

NELR lines were intermediate between those of the low-ionization lines and the broad Hβ on an object-by-object basis. The number of lines observed in each object was small, but they showed that a similar relationship might be present in both QSOs as well as Seyfert 1 systems. We have examined the mean ratio of the line widths of the [Fe VII] or [Ne V] lines to the [O III] λ5007 line for the objects in their sample and find that these ratios agree within errors with those expected from the mean slope of the AGN data presented in Table 4. Appenzeller & Wagner also found a weaker correlation between the line width of the [O III] λ5007 line and Hβ than is the case for the higher ionization forbidden lines. While this result appears, at first sight, to pose a problem for the continuous velocity field model, there are a number of reasons why [O III] may not accurately trace the velocity field in all objects. The presence of extended [O III] emission and/or reddening may mask the true line width of the nuclear emission line component. In particular, it has long been known that strong line emission is associated with radio jets (Whittle 1985). Most of the Appenzeller & Wagner QSO sample come from the Parkes radio-selected sample and radio measurements exist for a number of the Seyfert comparison sample. In at least some objects the gas associated with the [O III] emission may be subject to the galaxian gravitational potential rather than that of the nucleus. Quite detailed models have been developed to explain observational data on this basis, and the inclination angle of the emission-line regions to our line of sight may be responsible for apparent differences from object to object (Veilleux 1991).

6.4. *Correlation with Critical Density or Ionization Potential*

Previous studies of narrow emission lines (Filippenko & Halpern 1984; Filippenko 1985; Appenzeller & Östereicher 1988) have found evidence for a correlation between the line width of the narrow emission lines and the critical density, n_{crit}, for de-excitation of those lines. In addition, these studies have found evidence for a relationship between line width and ionization potential, χ. Determining whether the line width correlates better with n_{crit} or with χ is difficult for cases in which there is a difference in the ranges covered by the two independent variables as weaker correlations are to be expected for data with the smaller range when noise is present. However, with this in mind, in Table 4 we have compiled a list of objects showing a relationship between FWHM and n_{crit} in order to aid in analyzing the correlation seen in PG 2251+113. We have chosen these objects from a larger sample available in the literature with the requirement that the likelihood of the observed correlation between line width and critical density occurring by chance must be less than 1% (two-sided probability). To test the correlations we used the nonparametric Kendal τ test which has the advantage over the better known Spearman rank-order correlation coefficient in that it is generalizable to a partial coefficient (see, for example, Siegel & Castellan 1988). We have made use of this property to test the hypothesis that the line widths correlate better with χ than with n_{crit}. By using the partial rank correlation, we are able to factor out the contribution of the ionization potential and density independently to check which is stronger. We find that correlations with critical density are stronger (always >99%) than those with ionization potential (~97% for NGC 7213, but more typically <86%), lending support to density variation models in which density and velocity increase together in an inward direction.

While the observations do not suggest a preferred velocity field for the emission-line regions in PG 2251+113, we can speculate on possible correlations using a simple model. Consider the case of virial motion for which the velocity, v, of the gas clouds is proportional to $R^{-0.5}$, where R is the distance of a cloud from the central source. Such a velocity field holds to within a small factor for material in free fall, chaotic motion around the central source, or in Keplerian motion. To simplify matters further, we shall assume that the emitting clouds have a uniform ionization parameter. Support for both of these assumptions comes from the observations of the shape of line profiles with the similarity of line shapes in different objects (see, e.g., Whittle 1992, and references therein). A similar model was considered by Filippenko & Halpern (1984) in their study of the velocity field of the LINER NGC 7213.

For a photoionization model with constant ionization parameter the density, n, scales as $R^{-0.5}$ and, as the gas is virialized, we have FWHM $\propto n^{0.25}$. Support for gravitational dominance comes from studies of the correlation between host galaxy and emission-line properties for more general classes of object. Whittle (1992, and references therein) has shown that the [O III] λ5007 FWHM correlates well with estimated bulge masses for a variety of active galaxy types of the starburst, LINER, and Seyfert classes. For those objects in which the gas and stellar kinematics may be studied, there is reasonable agreement between the observed line width and that expected from the Faber-Jackson relationship, with offsets suggestive of differences in the mass-to-light ratio in the nuclear region. The conclusion of this work is that although the precise value of the central mass in differing classes of objects may not be sufficiently well predicted from host galaxy properties, the same general mechanism must be operating in all. Keplerian motion closer to the nuclear region has also been suggested by observations of a number of well-studied variable AGN (see Peterson 1993 for a recent review). In Table 4 we list the parameters of the least-squares fits to those objects showing a line width–critical density relationship. For these data the derived slopes are in good agreement with each other, but the weighted mean

TABLE 4

FITS TO THE FWHM–CRITICAL DENSITY RELATIONSHIP

Object	Number Lines	M_V	Slope	Intercept	n_e low	n_e high	r	Reference
PKS 1718−649	14	−19.1	0.144 ± 0.027	2.087 ± 0.163	5.0e3	3.3e7	0.840	1
NGC 3783	13	−20.2	0.134 ± 0.023	1.584 ± 0.131	5.0e3	1.0e10	0.869	2
Pic A	12	−20.7	0.095 ± 0.081	2.126 ± 0.081	2.0e3	3.3e7	0.907	1
NGC 7213	17	−20.8	0.200 ± 0.027	1.741 ± 0.155	2.0e3	3.3e7	0.889	3
Akn 120	8	−22.5	0.114 ± 0.012	2.055 ± 0.074	8.3e3	1.0e10	0.968	2
MR 2251−178	8	−23.7	0.138 ± 0.023	1.774 ± 0.148	1.0e4	3.3e7	0.929	1
2251+113	10	−25.8	0.113 ± 0.009	2.285 ± 0.077	5.0e3	1.6e11	0.969	4
Weighted mean			0.123 ± ~0.000					

REFERENCES FOR DATA.—(1) Filippenko 1985; (2) Appenzeller & Östereicher 1988; (3) Filippenko & Halpern 1984; (4) This work.

slope is only one-half of the value expected from the simple model described above. Clearly a more sophisticated model is called for.

7. CONCLUSIONS

The availability of *HST* FOS data has enabled us to study the line width–critical density relationship in PG 2251+113 in some detail and, for the first time, to show that the relationship holds not merely in the narrow and transition-line regions, but also in the BELR itself, which represents a range of over eight orders of magnitude in density. Although (by definition) the broad emission lines (including semiforbidden as well as permitted lines) are broader than the narrow lines, this is the first instance we know of in which UV and optical data have been combined to study the relationship between forbidden, semiforbidden, and permitted lines in a particular AGN. The connection between the BELR and the NELR is consistent with the statistical correlation found between FWHM([O III] λ5007) and FWHM(Hα) by Heckman, Miley, & Green (1984), but is contrary to the results found in individual objects by De Robertis & Osterbrock (1984) or Appenzeller & Wagner (1991). It is probable that there is a continuous range of properties from the BELR to NELR regions, but that other factors serve to mask these connections in some objects.

We have selected a biased sample of objects for study (see Table 4) which show a correlation between line width and density similar to that seen in PG 2251+113. The fits to the data for each object turn out to be very similar and are suggestive of a common origin. We have examined the possibility that the observed relationship between FWHM and critical density is due to the motion of the emission-line clouds in the gravitational potential of the central source. The derived dependence of the FWHM versus density relationship of $\approx n^{0.12}$ is a factor of $\sim$2 smaller than is predicted by a simple model of constant ionization parameter clouds orbiting in virial motion. Whittle (1992) has suggested that the kurtosis of observed [O III] λ5007 profiles suggests a velocity field in which FWHM $\propto R^{-0.1>\beta>-0.3}$. A velocity field of this type would result in a slope of $\sim$0.05–0.15 for the FWHM versus $n_{\rm crit}$ relationship under the assumption of constant ionization parameter throughout the line-emitting region. This range neatly brackets all but one of the observed values listed in Table 4. The "anomalous" value is that for NGC 7213 which also shows a strong correlation of line width with ionization potential (see § 6.4). The emission-line cloud properties in this object may differ from those of the others in our sample, perhaps through having variable column density across the emission-line regions (Veilleux 1991). Although the objects differ in luminosity and they span the range of types from LINER to QSO, we believe that the similarity of the derived relationship between line width and density points to a deeper similarity between these classes of objects. In addition, the run of properties for the narrow-line region in PG 2251+113 smoothly join those of the broad-line region at intermediate radii and suggests a continuity between these two regions. Although we have considered only the case of gravity-dominated, constant ionization emission-line zones, other models may fit the data more exactly. Detailed study of the line profile asymmetries and interline velocity shifts may clarify the issue.

The authors wish to express their thanks to Dr. Jerry Kriss for providing the SPECFIT package which significantly aided the emission-line analysis, to Drs. Todd Boroson and Giovanna Stirpe for providing spectra, and to S. Sherer for technical help and help with the preparation of the manuscript. Thanks are also due to Dr. Gary Ferland for making a copy of his photoionization code CLOUDY available and for answering numerous questions along the way. We would especially like to thank Dr. John Bahcall for comments on previous versions of the manuscript which significantly improved the text and for his organization of the Quasar Absorption Line Key Project as Principal Investigator. The anonymous referee is thanked for making suggestions which helped improve the paper. This research has made use of the NASA/IPAC Extragalactic Database (NED) which is operated by the Jet Propulsion Laboratory, California Institute of Technology, under contract with the National Aeronautics and Space Administration.

This work was partially supported by NASA contract NAG 5-1618 and grant GO-2424.01 from the Space Telescope Science Institute, and partial support for B. T. J. was provided by NASA through grant number HF-1045.01-93A from the Space Telescope Science Institute. The Space Telescope Science Institute is operated by the Association of Universities for Research in Astronomy, Inc., under NASA contract number NAS 5-2655.

REFERENCES

Angione, R. J., Moore, R. P., Roosen, R. G., & Stevens, J. 1981, AJ, 86, 653
Appenzeller, I., & Östereicher, R. 1988, AJ, 95, 45
Appenzeller, I., & Wagner, S. J. 1991, A&A, 250, 57
Bahcall, J. N., et al. 1993, ApJS, 87, 1
Boroson, T. A., & Green, R. F. 1992, ApJS, 80, 109
Burstein, D., & Heiles, C. 1978, ApJ, 225, 40
Carswell, R. F., Baldwin, J. A., Atwood, B., & Phillips, M. M. 1984, ApJ, 286, 464
Crampton, D., & Hutchings, J. B. 1990, AJ, 99, 37
De Robertis, M. M., & Osterbrock, D. E. 1984, ApJ, 286, 171
Diplas, A., & Savage, B. D. 1993, preprint
Drake, S. A., & Ulrich, R. K. 1980, ApJS, 42, 351
Falomo, R., Bersanelli, M., Bouchet, P., & Tanzi, E. G. 1993, AJ, 106, 11
Ferland, G. J. 1981, ApJ, 249, 17
Ferland, G. J., Peterson, B. M., Horne, K., Welsh, W. F., & Nahar, S. N. 1992, ApJ, 387, 95
Filippenko, A. V. 1985, ApJ, 289, 489
Filippenko, A. V., & Halpern, J. P. 1984, ApJ, 285, 458
Heckman, T. M., Miley, G. K., & Green, R. F. 1984, ApJ, 281, 525
Hutchings, J. B., & Neff, S. G. 1992, AJ, 104, 1
Kallman, T. R., Wilkes, B. J., Krolik, J. H., & Green, R. 1993, ApJ, 403, 45
Kriss, G. A. 1994, in Third Conference on Astrophysics Data Analysis and Software Systems, ed. D. Crabtree (ASP: San Francisco), in press
Lockman, F. J., & Savage B. D. 1993, in preparation
Marzini, P., & Sulentic, J. W. 1993, ApJ, 409, 612
Mathews, W. G., & Veilleux, S. 1989, ApJ, 336, 93
Netzer, H., & Laor, A. 1993, ApJ, 404, L51
Osterbrock, D. E. 1989, Astrophysics of Gaseous Nebulae and Active Galactic Nuclei (Mill Valley: University Science Books)
Pelat, D., Alloin, D., & Fosbury, R. 1981, MNRAS, 195, 787
Peterson, B. M. 1993, PASP, 105, 247
Phillips, M. M. 1978, ApJ, 226, 736
Pica, A. J., & Smith, A. G. 1983, ApJ, 272, 11
Rees, M. J., Netzer, H., & Ferland, G. J. 1989, ApJ, 347, 640
Savage, B. D., et al. 1993, ApJ, 413, 116
Schneider, D. P., et al. 1993, ApJS, 87, 45
Siegel, S., & Castellan, N. J. Jr. 1988, Nonparametric Statistics for the Behavorial Sciences (McGraw-Hill: New York)
Stirpe, G. 1990, A&AS, 85, 1049
Stockton, A., & MacKenty, J. W. 1987, ApJ, 316, 584
van Groningen, E. 1983, A&A, 126, 363
van Groningen, E., & de Bruyn, A. G. 1989, A&A, 211, 293
Veilleux, S. 1991, ApJ, 369, 331
Whittle, M. 1985, MNRAS, 215, 33
Whittle, M. 1992, Testing the AGN Paradigm (AIP: Conf. Proc. 254), 607
Wills, B. J., Netzer, H., & Wills, D. 1985, ApJ, 288, 94
Zheng, W. 1988, Astrophys. Lett. Comm., 27, 275
———. 1992, ApJ, 385, 127